Journal of the Indian Society of Remote Sensing (December 2018) 46(12):1939–1947
https://doi.org/10.1007/s12524-018-0857-0

RESEARCH ARTICLE

Sea-Level Change Over the China Sea and Its Vicinity Derived from 25-Year T/P Series Altimeter Data

Jianhua Wan[1,2] · Qinting Sun[1,2] · Shanwei Liu[1,2] · Yinlong Li[1,2]

Received: 27 June 2018 / Accepted: 8 October 2018 / Published online: 13 October 2018

Abstract

The characteristics of sea-level change in the China Sea and its vicinity are studied by combining TOPEX/Poseidon (T/P), Jason-1, Jason-2, and Jason-3 altimeter data. First, the sea-surface height is computed by using monthly data via collinear adjustment, regional selection, and crossover adjustment. The sea-level anomaly (SLA) from October 1992 to July 2017 is calculated based on the difference that is obtained by the value derived from the inverse distance weighting method to interpolate the CNES_CLS15 model value at a normal point. By analyzing the satellite data at the same time in orbit, three mean bias groups over the China Sea and its vicinity are obtained: the difference between T/P and Jason-1 is − 11.76 cm, the difference between Jason-1 and Jason-2 is 9.6 cm, and the difference between Jason-2 and Jason-3 is 2.42 cm. To establish an SLA series for 25 years in the study area, the SLAs are corrected. Mean rate of sea-level rise of the Bohai Sea, Yellow Sea, East China Sea, and South China Sea of 4.87 mm/a, 2.68 mm/a, 2.88 mm/a, and 4.67 mm/a, respectively, is found by analyzing the series of SLAs.

Keywords Satellite altimetry · China Sea · Sea-level anomaly · Rising rate

Introduction

The global climate has warmed in recent years, and this warming has caused a decrease in the extent of the polar ice sheets coincident with an increase in the sea level. Numerous disasters such as coastal erosion, saltwater intrusion, and flooding, all of which seriously threaten living environments and the safety of life and property worldwide, occur as a result of this sea-level rise (Bindoff et al. 2007). As a country with a coastline stretching 18,000 km, China's developed areas are mainly located throughout coastal regions. In recent years, an increasing number of studies have shown that the sea level along the coast of China has been rising under the background of a global sea-level increase (Wang et al. 2014; Zhang and Fang 2015). Therefore, it is necessary to strengthen research on sea-level changes over the China Sea and its vicinity.

Sea-surface height data obtained from tidal data have higher accuracies and longer time series (Douglas 2001). For example, Wu and others computed the average sea-level rise rate over 50 years with tidal data from the China Sea and its vicinity to be 1.3 ± 0.25 mm/a and determined the best fitting prediction method for the rate of sea-level rise (Wu et al. 2003). In addition, Chen and other scholars studied the seasonal variations and long-term trends in the sea level over the China Sea by using tidal data at 50 tide stations and determined an increasing sea-level rise rate in the China Sea which was 2.3 mm/a (Chen et al. 2008). However, traditional marine observation methods, such as coastal tide stations and ship measurements, have numerous disadvantages, including high costs, uneven

✉ Shanwei Liu
284920246@qq.com

Jianhua Wan
wjh66310@163.com

Qinting Sun
s16010068@s.upc.edu.cn

Yinlong Li
327423199@qq.com

[1] School of Geosciences, China University of Petroleum (East China), Huangdao 266580, Qingdao, China

[2] The Laboratory for Marine Mineral Resources, Qingdao National Laboratory for Marine Science and Technology, Qingdao 266071, China

measurement distributions, and long measurement periods. In contrast, satellite altimetry technology can be used to acquire large-scale observations of ocean information within a short time; therefore, satellite altimetry constitutes one of the most important methods used to study sea-level variations.

Since the first radar altimetry satellite Skylab was launched in 1973, large amounts of satellite altimeter data have been employed to research global sea-level change and the applications of other aspects related to marine science (Wang et al. 2004). For example, urban and others conducted research on global sea-level change using data from numerous sources; by combining altimeter data from the Geodynamics Experimental Ocean Satellite-3 (GEOS-3), SEASAT, GEOSAT, European Remote Sensing-1 (ERS-1), TOPEX/Poseidon (T/P), and ERS-2 satellites, they reported that the global rate of sea-level rise reached 3.3 ± 1.3 mm/a (Urban 2000). By analyzing altimetry data, another investigation indicated that sea-level change exhibits regional characteristics, that thermal expansion contributes substantially to sea-level rise, and that the global sea-level growth rate was 2.5 mm/a (Cazenave et al. 2003). Furthermore, Li and others established a uniform sea-surface height by using satellite altimeter data that had been calibrated with tidal station data and found that a global mean sea-level rise rate was 3.12 ± 0.4 mm/a over a period of approximately 18 years from 1993 to 2011 (Li et al. 2012). Research on sea-level changes throughout and surrounding the China Sea has been mainly accomplished by Chinese scientists. For example, a study conducted by Zhan and other scholars reported a signal with a period of 540 d in the South China Sea and East China Sea, and they found that mean sea-level rise rates for the East China Sea, Yellow Sea, and South China Sea were 4.61 ± 0.35 mm/a, 4.01 ± 0.49 mm/a, and 3.68 ± 0.41 mm/a, respectively (Zhan et al. 2008). Moreover, Sun and others reported that the sea-level rise rate in the vicinity of the China Sea was higher than the global rate (Sun et al. 2013). In addition, Guo and others studied the main cycle of sea-level change by using wavelet analysis and showed that El Niño and La Niña events have stronger effects on sea-level variations over the South China Sea than any other sea (Guo et al. 2015).

Jason-3 launched in 2016, and its orbit is identical to that of Jason-2 during its first few months of operation, and about 80 s apart from each other. In addition to T/P, Jason-1, and Jason-2, Jason-3 has provided 25 years of data with which to study sea-level changes, thereby ensuring the continuity of data. Jason-3 is the successor to the Jason-2 satellite; however, although these two satellites travel at a certain distance along almost identical orbits, there are some differences between their observations. Lauret and others found that the global bias between Jason-2 and Jason-3 was 2.99 cm (Lauret et al. 2017) and that the same group of satellites had different bias values in different sea areas. Accordingly, this article analyzes the biases between T/P and Jason-1, Jason-1 and Jason-2, and Jason-2 and Jason-3. Based on multigeneration satellite altimetry data from October 1992 to July 2017 and using the mean sea-surface MSS_CNES_CLS15 sea-level model, sea-level anomalies (SLAs) time series over the China Sea and its vicinity were established to study sea-level changes throughout various areas of the China Sea over the past 25 years.

Data Selection and Processing

Data Selection

The study area in this paper is composed of offshore China and its vicinity with an eastern longitude ranging from 105° to 135° and a latitude ranging from 0° to 45° (105°E–135°E, 0°N–45°N), as shown in Fig. 1. The satellite altimetry data employed herein are pretransitional geophysical data records (GDR) from the T/P, Jason-1, Jason-2, and Jason-3 satellites from October 1992 to July 2017 obtained from the French Space Center (CNES), and details regarding the data from these satellites are shown in Table 1. The MSS_CNES_CLS15 sea-level model utilized in this study is provided by the CNES and is recognized as a highly precise global sea-level model.

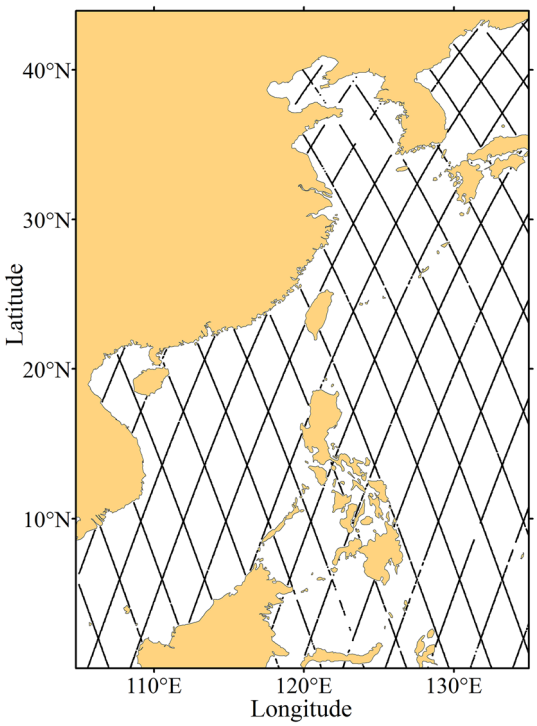

Fig. 1 Research area and tracks of satellites

Table 1 Altimetric data used to establish the SLA series

Altimetric data	Time span	Cycle
T/P	1992.10–2002.7	2–363
Jason-1	2002.1–2008.12	1–256
Jason-2	2008.7–2016.5	1–303
Jason-3	2016.2–2017.7	1–53

Data Processing

The GDR obtained from the T/P, Jason-1, Jason-2, and Jason-3 satellites are all characterized by low-quality data due to land, sea ice, and other factors; therefore, the original data were filtered to eliminate undesirable components. According to the editorial guidelines provided by CNES, land components, sea-ice targets, and contaminated data were removed first. Moreover, to obtain higher-quality altimetry data, it is necessary to correct for errors such as sea state deviations, atmospheric reverse pressures, and atmospheric refraction; thus, geophysical correction models described in the literature (Bronner et al. 2016; Dumont et al. 2017a, b) were employed to provide corrections for the data from the four satellites. Then, the data were processed by month.

One observation pass with the largest amount of valid data was selected as the reference pass from the same pass of multiple cycles as the reference pass, where each observation point along the reference pass is a normal point. Radial orbit errors and system errors in addition to the effects of temporal variations in repeated orbital period altimetric data were reduced based on collinear and crossover adjustments (Jiang et al. 2002). The sea-surface height of a normal point was obtained by the inverse distance weighting method. All SLA values of the normal points can be computed by using sea-surface height data along the normal point track minus the values calculated by interpolating the mean normal points within the sea-level model; however, due to the uneven distribution of survey points, the SLA values need to be weighted by the latitude (Ma 2014). The SLA time series for each month are shown in Fig. 2.

Results and Analysis

Data Analysis of Tandem Stages

The mean SLA time series of the China Seas based on the T/P, Jason-1, Jason-2 and Jason-3 altimetric data are shown in Fig. 2, from which it is evident that the SLA time series at the boundaries between the adjacent observation periods of two satellites do not exactly coincide. For example, in July 2002, the SLA obtained by using T/P satellite data was − 1.76 cm, while the SLA obtained by using Jason-1 data was 10.39 cm. Jason-1 follows the orbit of T/P almost identically with a separation of approximately 55 s; however, there are some differences in their measurements due to instrument errors and other factors. Therefore, the obtained SLA time series also have a certain deviation, which needs to be corrected. Similarly, the differences between Jason-1 and Jason-2 are very large, and there is also a certain deviation between Jason-2 and Jason-3. Therefore, these biases must be corrected. Accordingly, the data between T/P and Jason-1, Jason-1 and Jason-2, and Jason-2 and Jason-3 in their tandem stages (T/P cycles 344–363 correspond to Jason-1 cycles 001–020, Jason-1 cycles 240–259 correspond to Jason-2 cycles 001–020, and Jason-2 cycles 281–300 correspond to Jason-3 cycles 001–020) can be used to determine the biases between the SLA time series of adjacent satellites.

The following process is performed on the data between adjacent satellites in tandem stages. First, the SLA of each cycle was calculated based on the crossover adjustment and then averaged spatially. Second, the difference between satellites was computed based on the SLA difference between each cycle. Figure 3 shows the SLA between adjacent satellites in tandem stages before and after correction in the study areas. In addition, Table 2 shows the statistics regarding the differences between the four satellites before and after applying bias corrections.

The three left-hand graphs in Fig. 3 demonstrate that the SLA time series between T/P and Jason-1, Jason-1 and Jason-2, and Jason-2 and Jason-3 in their tandem stages possess obvious regularities. The data trends obtained by adjacent satellites in their tandem stages are exactly identical, and the differences between adjacent satellites fluctuate smoothly around a certain value. The differences between T/P and Jason-1 and between Jason-1 and Jason-2 are larger than that between Jason-2 and Jason-3. The difference between the maximum and minimum SLA between T/P and Jason-1 is 2.6 cm, that between Jason-1 and Jason-2 is 3.0 cm, and that between Jason-2 and Jason-3 is 1.4 cm. The observations from Jason-1 and Jason-2 fluctuate the most, while those from Jason-2 and Jason-3 fluctuate the least.

The three right-hand graphs in Fig. 3 demonstrate that the average difference is greatly reduced and the data continuity is greatly improved after correcting the biases. According to Table 2, prior to unifying the data, the mean difference in the SLA over 19 cycles determined between T/P and Jason-1 was − 11.76 cm; after unification, the average difference dropped to -4.7×10^{-8} cm. Similarly, the pre-unified average difference over 19 cycles

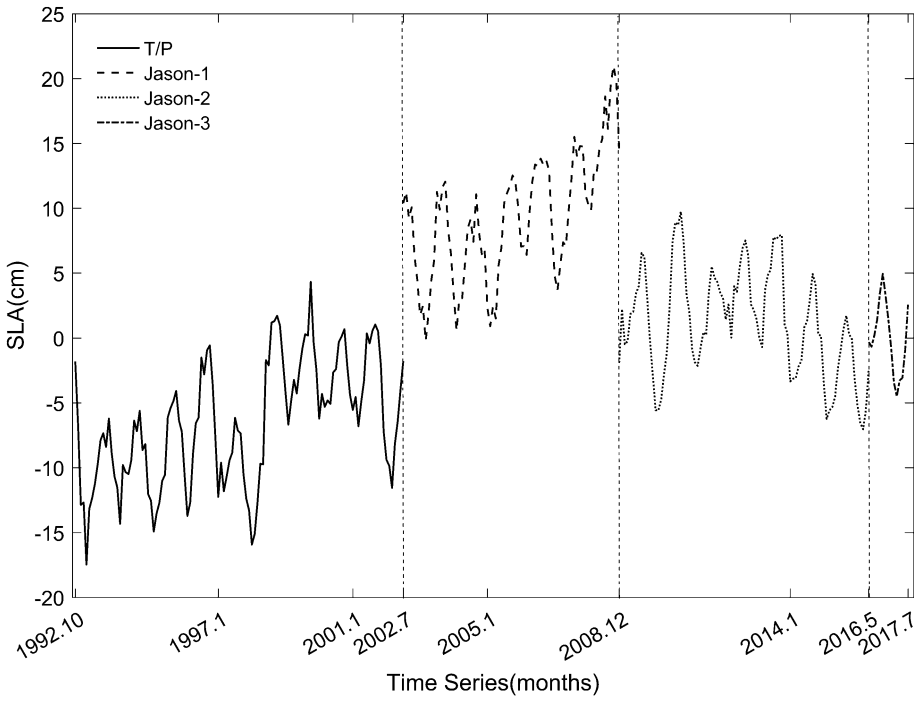

Fig. 2 Mean SLA time series of the China Seas

between Jason-1 and Jason-2 was 9.60 cm; after the data were unified, however, the average difference between these two satellites was reduced to 2.1×10^{-8} cm. The same difference between Jason-2 and Jason-3 was reduced from 2.42 cm to 9.4×10^{-17} cm.

The T/P satellite was used as a benchmark herein to apply a system bias correction to the Jason-1, Jason-2, and Jason-3 altimetric data; accordingly, the system errors were greatly reduced, and the data continuity was enhanced. In this paper, the SLA time series observed by Jason-1, Jason-2, and Jason-3 are consistent with those observed by T/P. The added correction necessary for the data from Jason-1 was − 11.76 cm, that for Jason-2 was − 2.16 cm, and that for Jason-3 was 0.26 cm. The global differences between T/P and Jason-1 and between Jason-1 and Jason-2 computed by Beckley et al. (2010) were − 8.34 cm and 13.14 cm, respectively; furthermore, their study reported great differences in terms of these biases caused by variability among the research areas. Subsequently, Guo et al. (2015) found that the differences between T/P and Jason-1 and between Jason-1 and Jason-2 were − 9.72 cm and 11.03 cm, respectively; certain differences in the results were attributed to error corrections or to the data processing scheme. Moreover, Sun et al. (2013) found that the SLA difference between Jason-1 and Jason-2 was − 7.33 cm, which is quite different from the difference of 9.60 cm calculated in this paper. This discrepancy is attributed to the fact that updated Jason-2 GDR-E data were used in this paper, whereas Jason-2 GDR-D data were used by Sun et al. (2013). The main changes between the previous GDR-D and the new GDR-E standards are updated geopotential models accounting for interannual variability, orbit parameterization, and orbits better referenced to the center of mass of the total Earth system.

The SLA time series in the tandem stages of each satellite pair were obtained after collinear and crossover adjustments, after which they were gridded. The mean SLA differences during the formation flight phase were obtained by computing the difference in the gridded SLA time series between adjacent satellites, and the results are shown in Fig. 4.

The three panels in Fig. 4 illustrate that the differences in the SLA vary among the different areas of the China Seas. Figure 4a reveals that the SLA differences between T/P and Jason-1 in the study area are generally negative; in addition, the differences are larger in coastal areas and in the north, whereas the differences in the middle of the China Sea are smaller than those in the south. Furthermore, Fig. 4b shows that the SLA differences between Jason-1 and Jason-2 are positive overall; the differences throughout the northern coastal areas are negative, and the differences in the southern sea area are distributed evenly. Figure 4c shows that the SLA differences between Jason-2 and Jason-3 are small throughout the study region, although the differences in the north are relatively large, and the distribution of differences in the other areas is relatively uniform. These findings confirm that the biases are attributable to differences among the geographical locations. It is therefore necessary to calculate a bias value for each area of the China Seas to improve the accuracy of the data. The

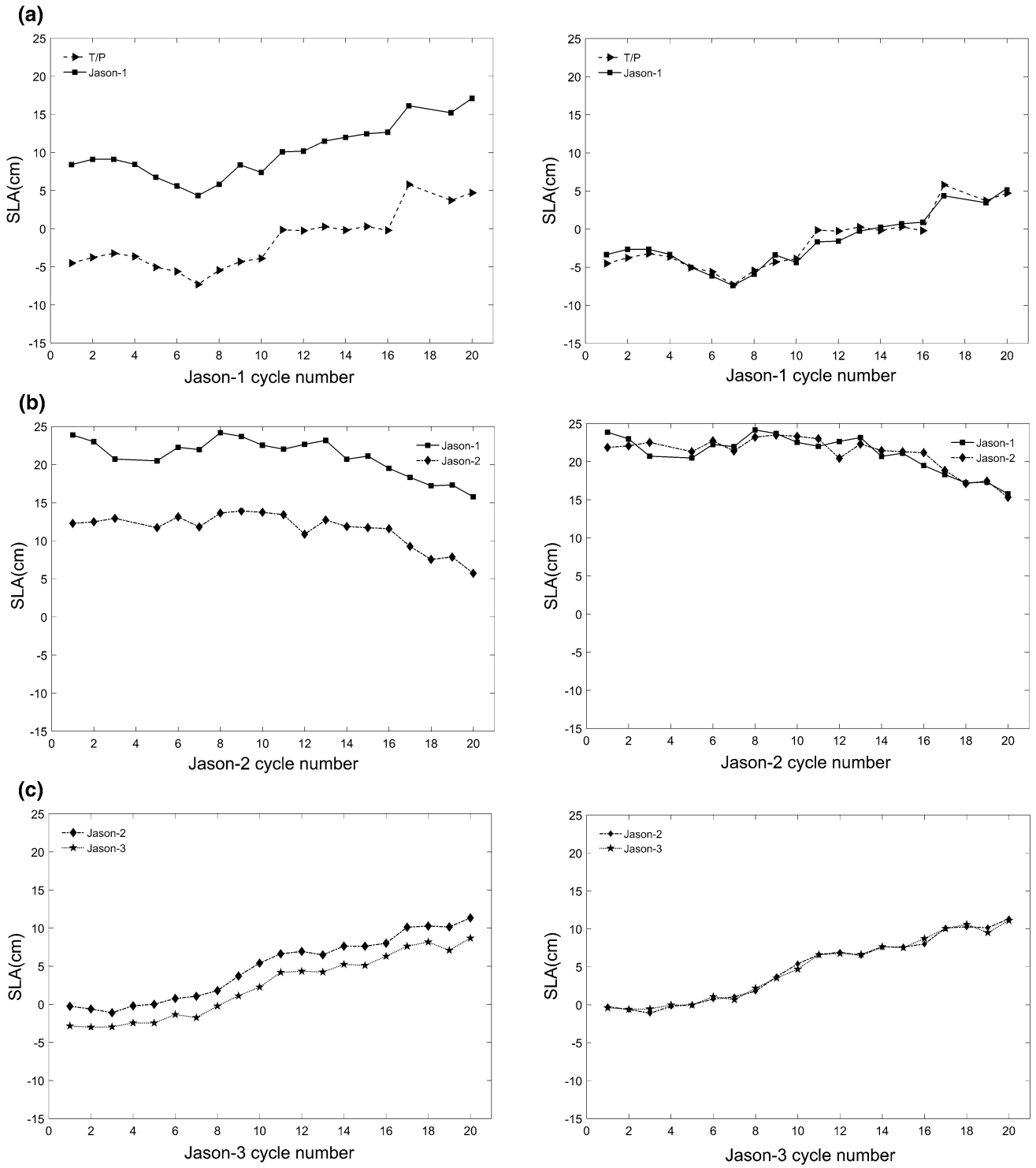

Fig. 3 Comparisons of the SLA time series among the four satellites in their tandem stages before and after correcting for deviations. **a** The SLA time series between T/P and Jason-1 in their tandem stages before and after correcting for deviations. **b** The SLA time series between Jason-1 and Jason-2 in their tandem stages before and after correcting for deviations. **c** The SLA time series between Jason-2 and Jason-3 in their tandem stages before and after correcting for deviations

approximate ranges of each sea area are as follows: Bohai Sea (117.5°–122°E, 37°–41°N), Yellow Sea (119°–126°E, 33°–37°N), East China Sea (120°–127°E, 23°–33°N), and South China Sea (110°–119°E, 14°–23°N). Table 3 shows the mean differences in the different sea areas.

Table 2 Statistics of the differences among the four satellites before and after bias corrections. Units: cm

	Difference	Differences after bias corrections
SLA(T/P)–SLA(Jason-1)	− 11.76	-4.7×10^{-8}
SLA(Jason-1)–SLA(Jason-2)	9.60	2.1×10^{-8}
SLA(Jason-2)–SLA(Jason-3)	2.42	9.4×10^{-17}

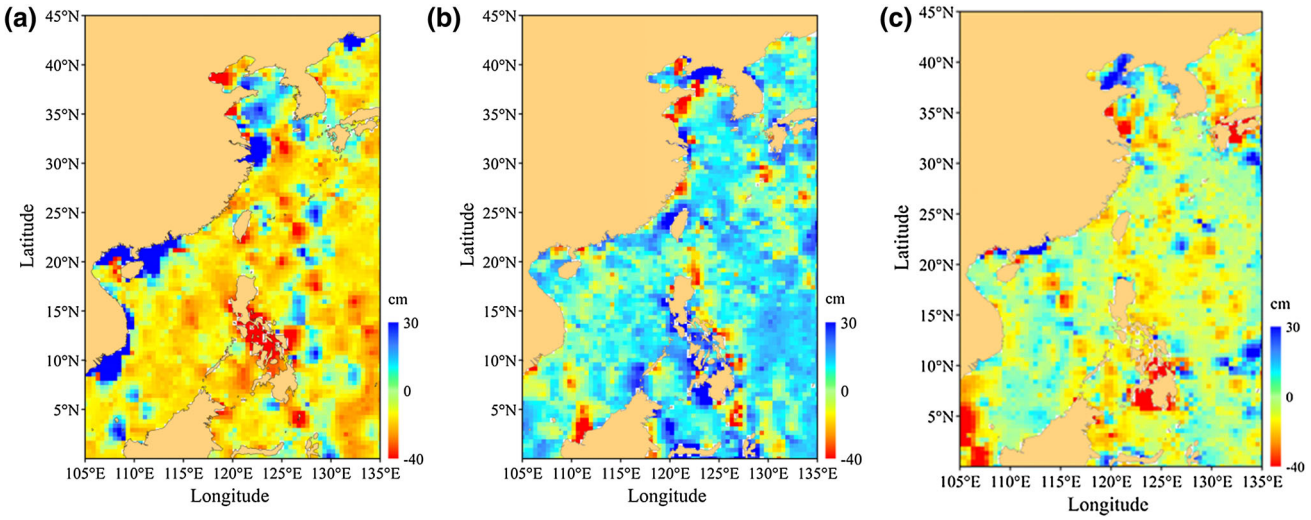

Fig. 4 SLA differences during the formation flight phase. **a** Mean SLA differences in the tandem stages between T/P and Jason-1. **b** Mean SLA differences in the tandem stages between Jason-1 and Jason-2. **c** Mean SLA differences in the tandem stages between Jason-2 and Jason-3

Table 3 Statistics of the mean differences in different sea areas. Units: cm

	T/P–Jason-1		Jason-1–Jason-2		Jason-2–Jason-3	
	Average difference	SD	Average difference	SD	Average difference	SD
Bohai Sea	− 9.57	10.73	8.42	5.20	2.94	1.94
Yellow Sea	− 12.32	2.47	9.78	2.86	2.65	1.16
East China Sea	− 12.72	2.96	10.00	2.40	2.80	0.84
South China Sea	− 11.64	2.84	11.49	2.05	2.19	0.78
Study area	− 11.76	0.87	9.60	1.20	2.42	0.36

Table 3 reveals great variability in the biases between the pairs of satellites over different sea areas. The SLA difference between T/P and Jason-1 in the Bohai Sea is − 9.57 cm, which is somewhat smaller than that for the overall study area (with an approximate 2-cm difference). Consequently, using the SLA difference for the entire study area would reduce the accuracy of the results. A large difference is also observed when comparing the biases between Jason-1 and Jason-2 in different areas with those for the study area. The difference between Jason-2 and Jason-3 is closer to the entire study area. In the Yellow Sea, the difference between the Jason-1 and Jason-2 satellites is quite different from that over the study area; in addition, the differences between T/P and Jason-1 and between Jason-2 and Jason-3 over the Yellow Sea are not as different from the entire study area. In the East China Sea, the SLA difference between the T/P and Jason-1 satellites differs from that in the entire study area by approximately 1 cm, and the differences between Jason-1 and Jason-2 and between Jason-2 and Jason-3 are very similar to those over the study area. In the South China Sea, the SLA differences have the highest degree of agreement with the differences over the study area, whereas the differences between the T/P and Jason-1 satellites are quite different in each sea area. Because the Bohai Sea is surrounded by land on three sides, the measured sea level therein is different the sea levels of other sea areas. The differences between the pairs of satellites are also greater with regard to the standard deviation in each sea area, especially in the Bohai Sea. The differences between Jason-1 and Jason-2 increase from north to south, and the Jason-2 and Jason-3 differences differ slightly in each sea area. The system error can be reduced by calculating the bias between each pair of

satellites in different sea areas, thereby making the results more continuous and accurate.

Sea-level Anomaly (SLA) Analysis

The SLA for the overall study area was corrected by correcting the biases and implementing linear fitting, as shown in Fig. 5. The sea-level rise rate for the study area was 3.96 mm/a. Moreover, the rate of sea-level increase along the coast of the China Sea (4.64 mm/a) was similar to that obtained by Guo et al. (2015).

Figure 5 clearly shows that the SLA in the study area exhibits an upward trend, and there is an obvious periodic variation pattern: The sea level decreases after the sea level rises in the summer and autumn and drops in the winter and spring. Since October 1992, the sea level has demonstrated a cyclical upward trend. In September 1997, the sea level dropped rapidly, and the SLA was the lowest in February 1998. This trend had a close relationship with the El Niño phenomenon from 1997 to 1998; then, it rapidly increased again. From 1999 to 2001, the sea level gradually increased. From 2002 to 2004, the overall trend showed upward characteristics, but the trend decreased relative to that from 1999 to 2001. The sea-level trend began to recover in 2005, and a rise occurred after a decline again in 2010. The sea level decreased from 2014 to 2016 and then began to rise again in 2017. In addition to the effects of tides, gravitational forces, and other factors, sea-level fluctuations are also greatly affected by large climate changes, such as those in 1997–1998, 2002–2003, 2004–2005, 2006–2007, 2009–2010, and 2014–2015, when El Niño phenomena occurred globally. Accordingly, the sea level has been affected to varying degrees, especially when a large El Niño phenomenon occurred from 1997 to 1998.

The Southern Oscillation Index (SOI) can effectively reflect the activity of the El Niño phenomenon. If the value of the SOI is consistently negative, there will be an El Niño phenomenon that year; if the value is consistently positive, there will be a La Niña event that year (Trenberth 1984). A comparison of the SOI index with the changes in the sea level is shown in Fig. 5, which clearly shows that the sea-level change trend is consistent with the change trend in the SOI index; in addition, the correlation coefficient between the SLA and SOI index is 0.32. Thus, there is a certain correlation between the changes in the sea level and El Niño phenomena.

The SLA of each sea area throughout the China Seas was obtained by using the SLA for the entire study area, after which the SLA was corrected by using the bias values in Table 3. Finally, the SLA time series for the various areas of the China Seas were obtained and analyzed. Least squares linear fitting was performed, and then, the SLA time series were compared with the SOI index, as shown in Fig. 6. Different sea areas have different SLA time series and rates of sea-level rise, which may be due to differences among the geographical locations, regional climate, and other factors. The mean rates of sea-level rise in the Bohai Sea, Yellow Sea, East China Sea, and South China Sea were 4.87 mm/a, 2.68 mm/a, 2.88 mm/a, and 4.67 mm/a, respectively.

Figure 6a shows that the greatest fluctuations in the SLA occurred in the Bohai Sea, where the difference between the maximum and minimum values was 96.35 cm. This is attributed to the geographical position of the Bohai Sea: The latitude of the Bohai Sea is higher than those of the

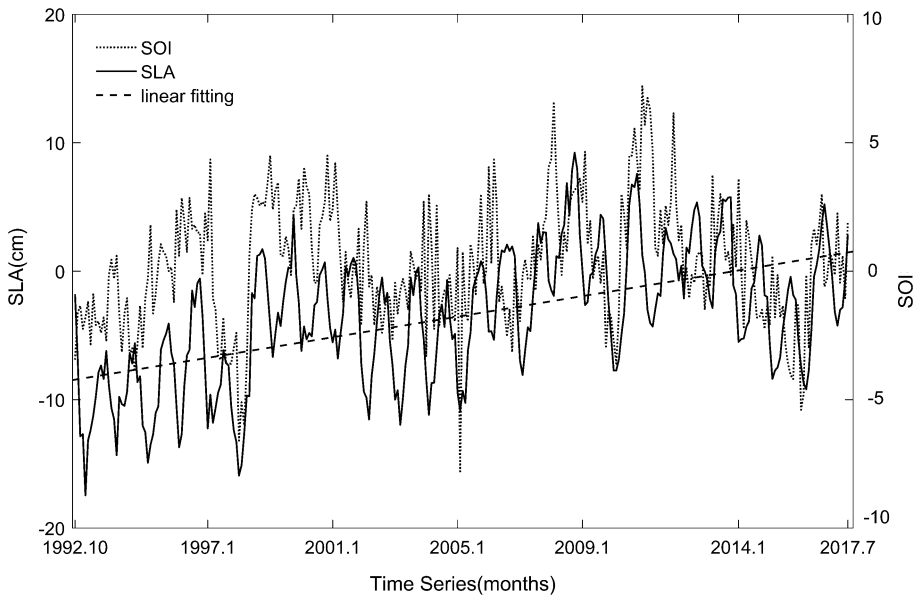

Fig. 5 Mean SLA time series of China seas after bias corrections

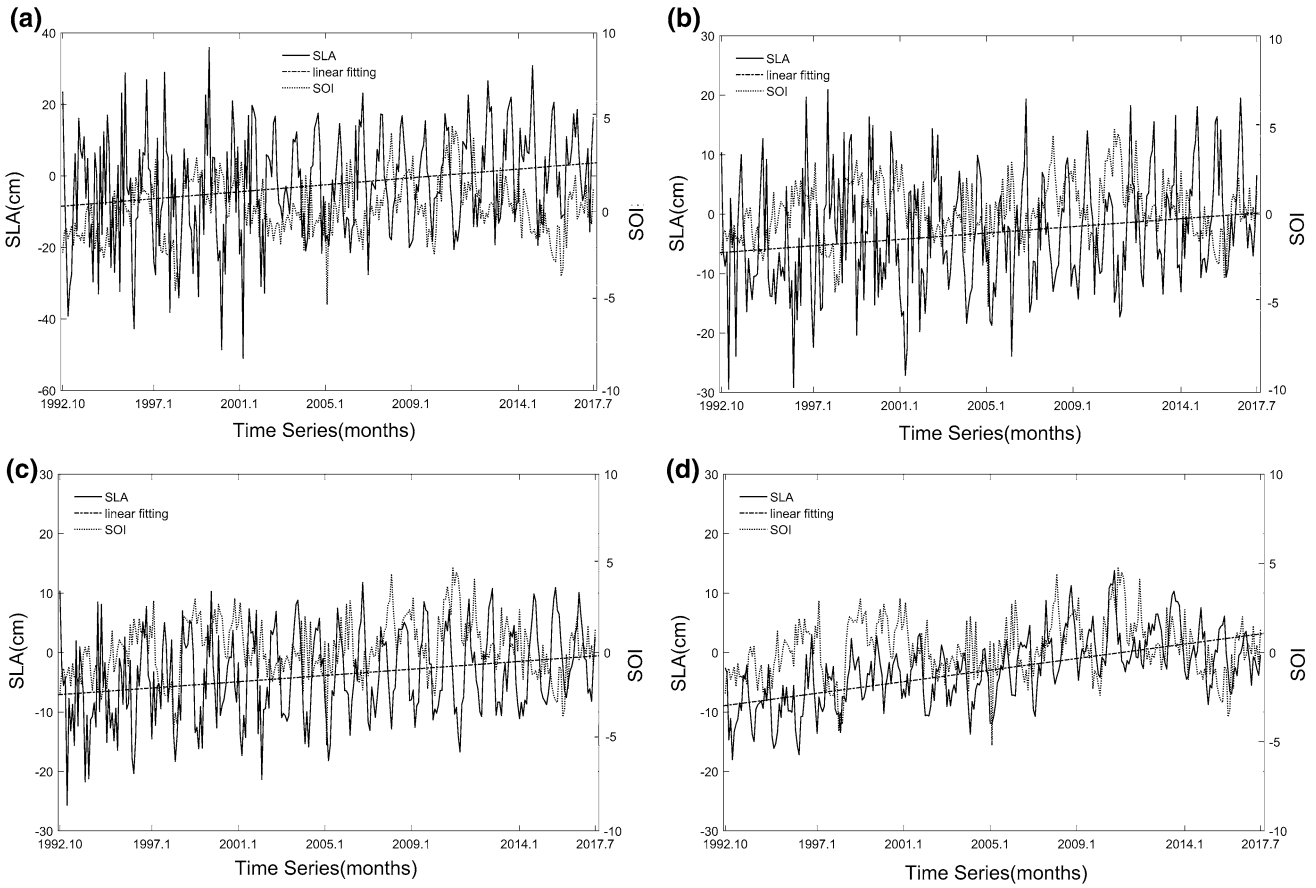

Fig. 6 Mean SLA time series for the China Seas after bias corrections. **a** The mean SLA time series for the Bohai Sea. **b** The mean SLA time series for the Yellow Sea. **c** The mean SLA time series for the East China Sea. **d** The mean SLA time series for the South China Sea

other sea areas, and it is surrounded by land on three sides. In addition, seasonal changes in the Bohai Sea are even more pronounced than those in other sea areas, and the seasonal variations in the SLA are larger. During the period from 1997 to 1999, during which an El Niño occurred, the SLA did not significantly change, indicating that the El Niño event had little impact on the Bohai Sea. From October 1992 to July 2002, the SLA of the T/P phase fluctuated largely, and the regularity was not obvious. Afterward, the SLA increased as a whole, and there was a sharp rise after a decline from 2006 to 2007.

The latitudes of the Yellow Sea and Bohai Sea are similar, and both seas exhibit relatively obvious seasonal changes. As seen in Fig. 6b, there was no obvious regularity in the periodicity of the T/P satellite data from the Yellow Sea region. In 1995, the SLA changed smoothly. The minimum SLA occurred in February 1996, and there were no significant changes from 1997 to 1999. In 2001, there was a significant increase and decrease, and the largest change, which occurred in 2006, was 44.13 cm.

Figure 6c shows that the interannual variations in the East China Sea region were more obvious. The SLA showed a steady upward trend overall. From 1992 to 1995, the SLA fluctuated greatly, and there was a significant increasing after decreasing in 2002.

Figure 6d shows that the change trend in the South China Sea and the change trend in the study area were the most consistent. The impact of El Niño phenomena was greater from 1997 to 1999. Moreover, the South China Sea had the smallest SLA fluctuations compared with the other sea areas; the difference between the maximum and minimum values in the South China Sea was 28.16 cm.

The correlation coefficients between the SOI and SLA in the Bohai Sea, Yellow Sea, East China Sea, and South China Sea were -0.10, -0.14, -0.03, and 0.23, respectively. Evidently, there is a certain correlation between El Niño and the SLA in the South China Sea. El Niño also has a certain impact on the SLA in the South China Sea, while it has smaller impacts on the other sea areas.

Conclusion

In this paper, 25 years of altimetry data from the T/P, Jason-1, Jason-2, and Jason-3 observation satellites from October 1992 to July 2017 were used to analyze the SLA time series in the China Sea and its vicinity. The conclusions drawn from these data are as follows:

1. There are certain biases among the T/P series satellites that need to be corrected by using the data in tandem stages. The difference between T/P and Jason-1 was − 11.76 cm, while that between Jason-1 and Jason-2 was 9.6 cm and that between Jason-2 and Jason-3 was 2.42 cm.
2. The SLA of the China Sea and its vicinity is increasing, and the various areas are characterized by different sea-level rise rates. The 25-year SLA time series were linearly fitted; the corresponding mean sea-level rise rates in the Bohai Sea, Yellow Sea, East China Sea, and South China Sea were 4.87 mm/a, 2.68 mm/a, 2.88 mm/a, and 4.67 mm/a, respectively. The sea-level rise rates (from high to low) are as follows: Bohai Sea, South China Sea, East China Sea, and Yellow Sea.

Acknowledgements The authors wish to thank the editor. The authors also thank the AVSO website of the French Space Center (CNES) for providing the satellite data and the National Oceanic and Atmospheric Administration (NOAA) for SOI data. This research has been supported by the National Key R&D Program of China (2016YFC1401800), Key R&D Program of Shandong Province (2018GHY115046), the Fundamental Research Funds for the Central Universities (17CX02071), NSFC (61571009), and National Programme on Global Change and Air-Sea Interaction (GASI-02-PAC-YGST2-04, GASI-02-IND-YGST2-04, GASI-02-SCS-YGST2-04).

References

Beckley, B. D., Zelensky, N. P., Holmes, S. A., et al. (2010). Assessment of the Jason-2 Extension to the TOPEX/Poseidon, Jason-1 Sea-Surface Height Time Series for Global Mean Sea Level Monitoring. *Marine Geodesy, 33*(S1), 447–471.

Bindoff, N., Willebrand, J., Artale, V., et al. (2007). Observations: Oceanic climate change and sea level. In S. Solomon, D. Qin, M. Manning, et al. (Eds.), *Climate change 2007: The physical science basis. Contribution of working group 1 to the fourth assessment report of the intergovernmental panel on climate change* (pp. 385–432). Cambridge: Cambridge University Press.

Bronner, E., Picot, N., Desjonqueres, J.D., et al. (2016). Jason-1 Products Handbook. https://www.aviso.altimetry.fr/fileadmin/documents/data/tools/hdbk_j1_gdr.pdf.

Cazenave, A., Nerem, R. S., Dominh, K., et al. (2003). Present-Day sea level change: Observations and causes. *Space Science Reviews, 108*(1–2), 131–144.

Chen, M.C., Zuo, J.C., Chen, M.X., et al. (2008). Spatial distribution of sea level trend and annual range in the China Seas from 50 long term tidal gauge station data. In *The proceedings of the eighteenth (2008) international offshore and polar engineering conference (ISOPE-2008)* (pp. 583–587).

Douglas, B. C. (2001). Sea level change in the era of the recording tide gauge. In B. C. Douglas, M. S. Kearney, & S. P. Leatherman (Eds.), *Sea level rise: History and consequences* (pp. 37–64). Cambridge: Academic Press.

Dumont, J.P., Rosmorduc, V., Carrere, L., et al. (2017a). OSTM/Jason-2 Products Handbook. https://www.aviso.altimetry.fr/fileadmin/documents/data/tools/hdbk_j2.pdf.

Dumont, J.P., Rosmorduc, V., Carrere, L., et al. (2017b). Jason-3 Products Handbook. https://www.aviso.altimetry.fr/fileadmin/documents/data/tools/hdbk_j3.pdf.

Guo, J. Y., Wang, J. B., Hu, Z. B., et al. (2015). Temporal-spatial variations of sea level over China seas derived from altimeter data of TOPEX/Poseidon, Jason-1 and Jsaon-2 from 1993 to 2012. *Chinese Journal of Geophysics, 58*(9), 3104–3120.

Jiang, W. P., Li, J. C., & Wang, Z. T. (2002). Combining multi-satellite data to compute the global average sea surface WHU2000. *Chinese Science Bulletin, 47*(15), 1187–1191.

Lauret, O., Philipps, S., & Lievin, M. (2017). Jason 3 validation and cross-calibration activities (Annual Report 2016).

Li, D. W., Li, J. C., Jin, T. Y., et al. (2012). Monitoring global sea level change from 1993 to 2011 using TOPEX and Jason altimeter missions. *Geomatics and Information Science of Wuhan University, 37*(12), 1421–1424.

Ma, L. B. (2014). Spatiotemporal features and possible mechanisms of seasonal changes in sea surface height south of Japan. *Chinese Journal of Oceanology and Limnology, 32*(4), 933–945.

Sun, W., Wang, Q. B., & Zhu, Z. D. (2013). Sea level anomaly series in China sea and ite vicinity based on multi-generation satellite altimetric data. *Acta Geodaetica et Cartographica Sinica, 42*(4), 494–500.

Trenberth, K. E. (1984). Signal versus noise in the Southern Oscillation. *Monthly Weather Review, 112*(2), 326–333.

Urban, T. J. (2000). *The integration and application of multi-satellite radar altimetry*. Austin: University of Texas.

Wang, H., Liu, K. X., Fan, W. J., et al. (2014). Analysis on the sea level anomaly high of 2012 in China coastal area. *Acta Oceanologica Sinica, 36*(5), 8–17.

Wang, Z. T., Li, J. C., & Chao, D. B. (2004). Correlativity study between El Niño phenomenon and mean sea level abnormal variations in equator pacific area using multi-satellite altimetric data. *Geomatics and Information Science of Wuhan University, 28*(9), 699–703.

Wu, Z. D., Li, Z. Q., & Zhao, M. C. (2003). The process and prediction of sea level change of China offshore waters in 50 years. *Hydrographic Surveying and Charting, 23*(2), 17–19.

Zhan, J. G., Wang, Y., Xu, H. Z., et al. (2008). The wavelet analysis of sea level change in China sea during 1992–2006. *Acta Geodaetica et Cartographica Sinica, 37*(4), 438–443.

Zhang, J., & Fang, M. Q. (2015). Sea level trends of China seas from 1993 to 2012. *Periodical of Ocean University of China, 45*(1), 121–126.